

# Inverse Designed Grating Coupler With Low Loss and High Bandwidth on LNOI Platform

Xingsheng He , Dongyue Sun , Jingye Chen , and Yaocheng Shi

**Abstract**—A grating coupler structure on a X-cut lithium niobate on insulator (LNOI) platform is designed and demonstrated. The utilized inverse design method is based on gradient-based adjoint optimization method, which is time saving and with more optimization degrees of freedom. For TE polarization, the high coupling efficiency of  $-3.3$  dB is experimentally obtained. The maximum coupling efficiency is still  $-3.9$  dB with the broadband 3-dB bandwidth of 90 nm. The grating coupler of high performance is realized by only single step etching and without bottom metal reflection layer.

**Index Terms**—Grating coupler, lithium niobate, inverse design.

## I. INTRODUCTION

LITHIUM niobate on insulator (LNOI) has excellent optical properties, including wide transparent windows from visible light to mid-infrared [1] and other nonlinear optical properties such as electro-optic, acousto-optic, photorefractive and piezoelectric. It is compatible with semiconductor processing technology and is becoming one of the key platforms for integrated photon technology [2], [3], [4]. A series of high-performance LNOI integrated optical devices have been developed, such as tunable frequency combs [5], [6], [7] and high-frequency and low-voltage electro-optic modulators [8], [9]. However, there is a critical problem in fiber coupling with off-chip light sources and detectors for all LNOI devices. However, unlike thick films and bulk materials, high efficiency coupling between the LNOI waveguide and a single-mode fiber is relatively difficult because the mismatch between the waveguide mode and the fiber mode is obvious. At present, the common coupling approaches are divided into two kinds: end-face coupling and grating coupling. End-face coupling, such as reverse taper [10], tapered fiber [11], [12], [13], [14] and lenticular fiber [15], [16], can realize optical coupling with low loss, wide band and low polarization dependence, but the input and output ports are limited to the edge of the chip,

requiring strict post-manufacturing processing such as edge polishing and high-resolution optical alignment. The design and manufacturing process of end-face coupler on LNOI platform becomes more complex, often requiring multi-step etching or special cladding [17] to further expand the size of on-chip mode field. In contrast, grating couplers provide chip surface solutions that can be placed anywhere on the wafer/chip, be easier to align, have lower manufacturing costs. To improve the coupling efficiency and bandwidth, several works have been done to improve the efficiency of LNOI grating couplers, such as chirped and apodized structure [18], [19], bottom metal reflection layers [18], [20], and top deposition [21], [22]. Although the former could improve the peak efficiency of the device, the optimization results often fail to account for bandwidth, while the latter two greatly increase the complexity and cost of the process. Meanwhile, these optimizations usually start with standard designs and rely on parameter scanning, random perturbation, or population-based meta-heuristic algorithms such as genetic algorithms and particle swarm optimization. Owing to their derivative-free properties, optimization degrees-of-freedom are often limited to a few parameters and time-consuming.

In this paper, we demonstrate a series of grating couplers that balance coupling efficiency and coupling bandwidth in the 400 nm X-cut LNOI. The inverse design method is based on gradient-based adjoint optimization method, which is time saving and with more optimization degrees of freedom [23], [24], [25], [26], [27]. Different designs for different target bandwidths show the desired performance in the experiment. The experimental results show that the maximum coupling efficiency of TE polarization is  $-3.3$  dB. The peak coupling efficiency can reach  $-3.9$  dB when the TE polarization 3-dB bandwidth is 90 nm. Compared with traditional couplers on LNOI platform, our proposed grating coupler is of high performance and can be realized by only single step etching and without bottom metal reflection layer.

## II. THEORY AND DESIGN

The grating coupler is designed on the 400 nm X-cut LNOI platform, under which a 3  $\mu\text{m}$ -thick  $\text{SiO}_2$  layer is buried. The grating schematic diagram is shown in Fig. 1, and the grating number is set to 20, which is enough to cover the entire single-mode optical fiber spot size. Fig. 1(c) shows the coupling of grating waveguide mode to fiber mode.

The inverse design method based on gradient does not rely on parameter scanning or random perturbation to find the minimum values. And the adjoint method is used to obtain the field

Manuscript received 7 October 2023; revised 21 December 2023; accepted 4 January 2024. Date of publication 9 January 2024; date of current version 24 January 2024. This work was supported in part by the National Major Research and Development Program under Grant 2021YFB2801703, in part by the National Natural Science Foundation of China under Grants 62135011 and 62105286, in part by “Pioneer” and “Leading Goose” R&D Program of Zhejiang under Grant 2022C01103, in part by Ningbo Natural Science Foundation under Grant 2023J282, and in part by the Fundamental Research Funds for the Central Universities. (*Corresponding author: Jingye Chen.*)

The authors are with the State Key Laboratory for Modern Optical Instrumentation, Center for Optical and Electromagnetic Research, Ningbo Innovation Center, College of Optical Science and Engineering, Zhejiang University, Zhejiang 310027, China (e-mail: jingyechen@zju.edu.cn).

Digital Object Identifier 10.1109/JPHOT.2024.3351199

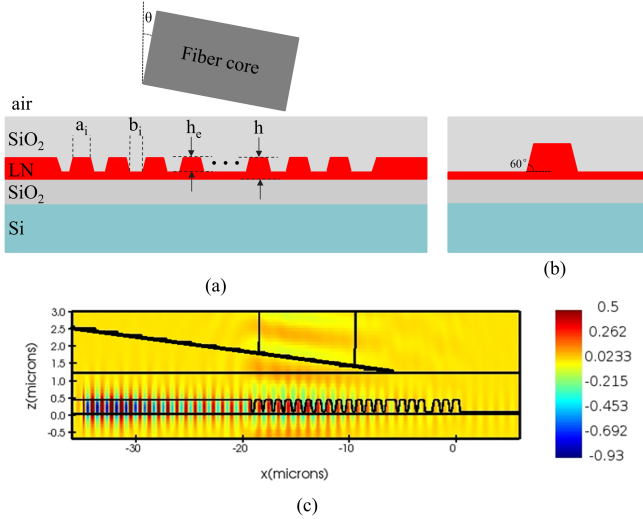


Fig. 1. (a) Schematic diagram of the grating coupler on LNOI, (b) cross section view, and (c) the diagram of coupling of grating waveguide mode to fiber mode.

distribution from the forward and “reverse” adjoint simulation respectively to calculate the gradient of the field distribution relative to the structure vector [28], which requires less simulation time than the genetic algorithm or particle swarm optimization. The typically numerical optimization problem of nanophotonic for grating couplers is as follows [31]:

$$\begin{aligned} & \min_{A, E} \sum_i T_i(E) \\ & \text{Subject to } \nabla \times \frac{1}{\mu_0} \nabla \times E - \omega^2 \in (A) E + i\omega J = 0, \\ & \quad i = 1, 2, \dots, n \end{aligned}$$

where  $T_i$  is the objective function,  $n$  is the number of objective functions,  $E$  is the electric field at  $\omega$ ,  $\epsilon(A)$  is the permittivity,  $J$  is source field, and  $A$  is vector that parametrizes the structure. For grating couplers,  $T_i$  is equal to the coupling efficiency from the source into the fundamental waveguide mode. Furthermore,  $T_i$  can also be extended to multi-objective problem such as low back reflection or polarization insensitivity by adjusting the objective function accordingly.

The flow chart of design is shown in the Fig. 2. In the optimization, due to the particularity of grating structure, we choose to directly adopt the envelope defined grating structure formed by the discrete parameter vector  $A = [a_1, b_1; a_2, b_2; \dots; a_n, b_n]$ , which corresponds to silicon oxide ( $\text{SiO}_2$ ) cladding and fiber outside the envelope, and lithium niobate within the envelope, where  $a_i, b_i$  ( $i = 1, 2, \dots, n$ ) is the length of the unetched and etched regions of the  $i$ -order grating, and the feature size constraint ( $a_i \geq 100 \text{ nm}, b_i \geq 0$ ) is applied to facilitate actual manufacturing and processing. In simulation, the sidewall wedge angle is set to  $60^\circ$  according to the fabrication. At the same time, the auxiliary vector  $B = [\theta, h_e]$ , where  $\theta$  is the incidence angle of the fiber, and  $h_e$  is the etching depth, is added to optimize the incident angle of the fiber and the etching depth to obtain a large coupling efficiency. In addition, in order to balance the

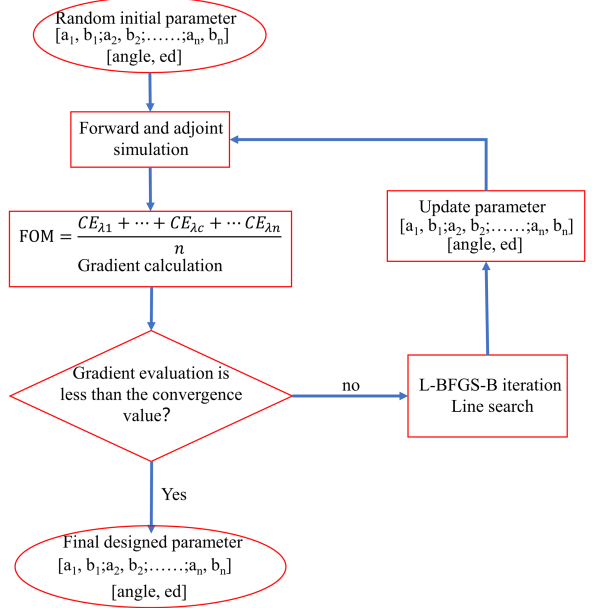


Fig. 2. Diagram of reverse design flow.

relationship between the coupling efficiency and bandwidth, the objective function is adjusted to the average coupling efficiency at equal interval wavelength. The L-BFGS-B algorithm is used for iteration until the optimal convergence.

A series of grating couplers are optimized at the center wavelength of 1550 nm and the 3-dB bandwidth of 40 nm, 60 nm, 80 nm, and 100 nm as targets, respectively. The interval wavelength is set to 10 nm, and the incident fiber is a single-mode fiber with a core of  $9 \mu\text{m}$  and a cladding diameter of  $125 \mu\text{m}$ . Due to the high computational cost of optimizing full 3D grating coupler, finite difference time domain (FDTD) is used for 2D simulation, and the number of optimization iteration is set to 150. Optimized for 40 nm 3-dB bandwidth, the optimal optical fiber angle is about  $2.5^\circ$  and the etching depth is about 280 nm. In order to unify subsequent processes and experimental tests, the incident angle and etching depth are constant for the other bandwidth optimizations. The optimized structural parameters are shown in Table I.

In order to further illustrate the results, we verify the optimization results by using 3D-FDTD, considering two kinds of structures: rectangular grating (as shown in Fig. 3(b) and (d)) and curved grating (as shown in Fig. 3(c) and (d)). Fig. 3(a) shows a schematic diagram of both structures. Optimization results of smaller target bandwidth usually exceed the target. This is because achieving small bandwidth does not sacrifice much for efficiency, and it is unrealistic to sacrifice bandwidth indefinitely for efficiency. At target of 100 nm bandwidth, the optimization results do not achieve the expected performance, which is attributed to the small angle of the fiber. Moreover, curved grating has larger bandwidth than rectangle and is close to 100 nm bandwidth in the case of target of 100 nm bandwidth. To characterize the effect of manufacturing error on device performance, we have calculated the effects of waveguide width and etch depth on the performance of type I grating. As shown

TABLE I  
OPTIMIZED STRUCTURAL PARAMETERS OF FOUR TYPES OF GRATINGS

Grating order	1	2	3	4	5	6	7	8	9	10	11	12	13	14	15	16	17	18	19	20	
Type I	a/nm	590	637	551	508	462	429	418	421	423	434	458	460	469	900	491	498	485	493	497	552
	b/nm	0	0	23	95	140	181	217	206	204	196	171	136	129	150	64	65	82	577	91	85
Type II	a/nm	565	689	339	354	351	339	367	383	407	428	436	452	455	467	473	468	501	494	482	553
	b/nm	0	13	187	252	281	298	296	252	234	209	178	162	140	132	117	111	577	94	90	102
Type III	a/nm	581	688	323	325	323	325	365	387	407	429	436	445	447	457	462	461	900	448	505	575
	b/nm	0	0	210	284	305	317	310	254	228	207	177	166	152	144	133	122	132	128	119	153
Type IV	a/nm	572	695	324	309	308	315	368	393	410	427	434	437	443	452	458	458	479	483	480	508
	b/nm	0	0	204	296	319	329	313	246	217	202	176	168	162	154	144	141	151	156	150	162

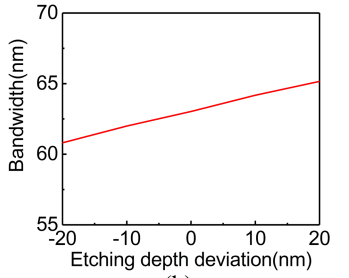
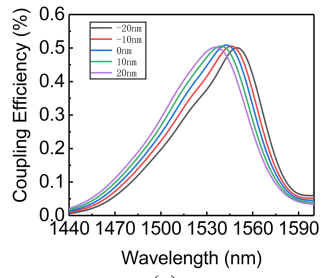
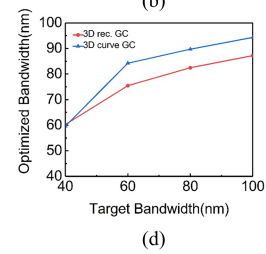
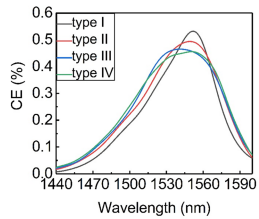
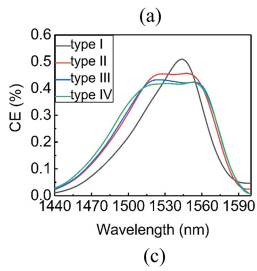
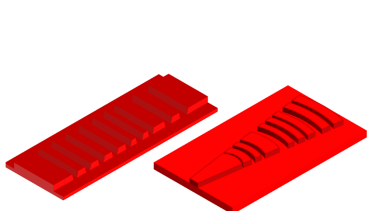


Fig. 3. (a) Schematic diagram of structures, (b) 3D rectangular grating verification, (c) 3D curved grating verification, (d) optimization results and target bandwidth.

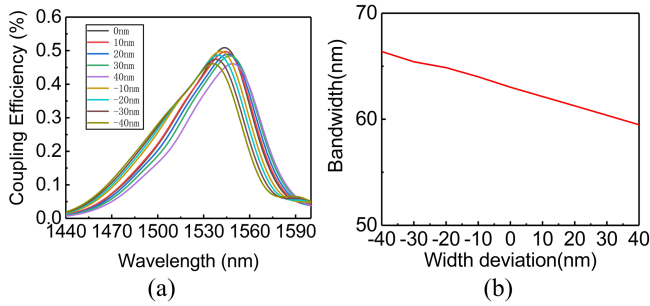


Fig. 4. (a) Coupling efficiency and (b) bandwidth varies with width deviation.

In Figs. 4 and 5, we can find that the coupling efficiency remains above 45% within the width deviation of  $\pm 40$  nm, and the bandwidth varies within  $\pm 4$  nm. When the etching depth deviation is of  $\pm 20$  nm, the coupling efficiency is affected little, and the bandwidth varies within  $\pm 3$  nm. In order to characterize the polarization dependence of the grating, we show the coupling

Fig. 5. (a) Coupling efficiency and (b) bandwidth varies with etching depth deviation.

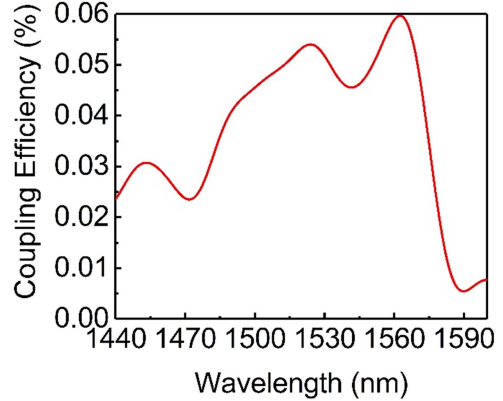


Fig. 6. Coupling efficiency of TM mode (type I).

efficiency of TM mode of grating type I in Fig. 6. It can be seen that the coupling efficiency of the designed grating in TM mode is less than 6% and the polarization correlation is good.

### III. FABRICATION AND MEASUREMENT

In the experiment, a series of curved grating couplers working at TE polarization are fabricated on x-cut LNOI platform. The height of the LN membrane is 400 nm. Images of optical microscope and scanning electron microscope (SEM) are shown in

TABLE II  
PERFORMANCE COMPARISON OF SOME REPORTED GRATING COUPLERS ON LNOI

Design structure	Simulated CE (dB)	Measured CE (dB)	Bandwidth (nm)	Fabrication process
Chirped GC[29]	-2	-3.6	48	EBL+ICP-RIE( $\text{Ar}^+$ )
Straight and curved GC with metal bottom layer [20]	-3.5	-3.1	/	EBL + Lift-off + RIE
Chirped and apodized GC with metal reflector [19]	-1.8(-0.8)	-6.9(-5.5)	90(82)	FIB etching
Metal deposition rec. GC[22]	-3	-3.58	58	EBL+ICP-RIE+ Lift-off
Deep etched with taper structure[30]	-3.6	-6.7	90	$\alpha\text{-Si}$ mask+ ICP-RIE( $\text{Ar}^+$ )
Metal deposition rec. GC [21]	-3	-3.56	/	EBL+ICP-RIE+ Lift-off
<b>Our work</b>	<b>-2.75</b> <b>-3.74</b>	<b>-3.37</b> <b>-3.9</b>	<b>75</b> <b>90</b>	<b>EBL+ICP-RIE(<math>\text{Ar}^+</math>)</b>

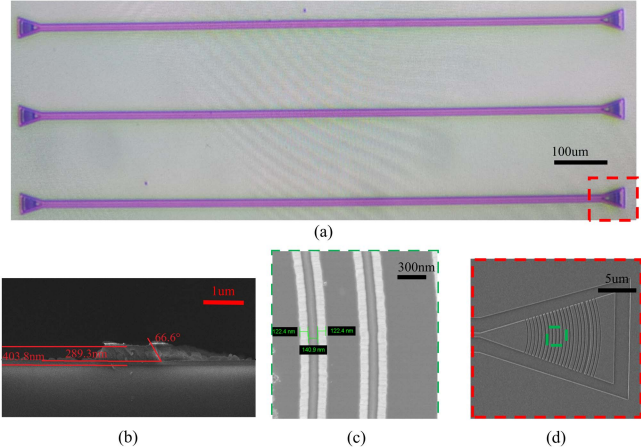


Fig. 7. (a) Microscope image, SEM image of (b)straight waveguide cross section, (c) grating local amplification, and (d) fabricated grating coupler.

Fig. 7. There is only single electron exposure and single etching step. The positive photoresist (ZEP 520A) is patterned by 50 keV electron beam lithography (EBL) and developed using amyl acetate. A low pressure argon plasma is used to transfer the pattern into the LN thin film by an ICP-RIE etching. Finally,  $\text{SiO}_2$  deposited by PECVD is used as the upper cladding. For characterization, each structure group consists of two grating couplers, one of which is used as an input coupler and the other as an output coupler. The couplers on both sides are connected by 1  $\mu\text{m}$ -wide waveguide to achieve single-mode transmission. The partial microscope image of the fabricated device is shown in Fig. 7(a). The SEM image of the grating coupler is shown in Fig. 7(d). Fig. 7(b) and (c) show the SEM image of the straight waveguide section and the enlarged view of the grating. The sidewall angle of the waveguide is about 66.6°.

The device characterization is performed in an optical fiber input/output measuring system. The measurements are made by two single-mode optical fibers, which are tilted up symmetrically at the angle of 2.5° as the input fiber and the output fiber. The supercontinuum spectrum is used as a source, and a polarizer and polarization controller are connected before the input fiber

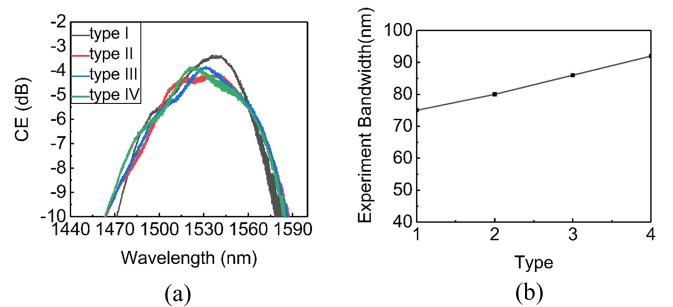


Fig. 8. Measured result of the fabricated grating coupler. (a) The coupling efficiency and (b) the bandwidth.

to ensure TE polarization input. To evaluate the coupling efficiency of each grating coupler, we normalize the recorded transmission spectra by measuring the laser spectrum as a function of wavelength and assume that the two grating couplers behave identically. The measured transmission spectra of TE mode is shown in Fig. 8. There are some differences between simulated and measurement results, which could be attributed to inevitable manufacturing errors in the fabrication process. At 1550 nm wavelength, the maximum coupling efficiency of TE polarization can reach  $-3.3$  dB, and the 3-dB bandwidth is 78 nm, of which the efficiency is slightly decreased but the bandwidth is increased compared with simulation results. The measured spectra agree well with the simulated ones. The grating optimized for a larger target bandwidth shows a larger measured bandwidth. The maximum coupling efficiency is still  $-3.9$  dB with the 3-dB bandwidth of 90 nm. Thus, our proposed device has performance of low loss and large bandwidth compared with representatively reported grating couplers on LNOI, as shown in Table II.

#### IV. DISCUSSION

In summary, we design and demonstrate a series of grating couplers on LNOI platform, taking into account both coupling efficiency and coupling bandwidth. We experimentally obtain high efficiency coupling of  $-3.3$  dB ( $-3.9$  dB) and

3-dB bandwidth of 78 nm (90 nm) at 1550 nm wavelength band, in the case of single step etching and without bottom metal reflector. In addition, the inverse design method is based on gradient-based adjoint optimization method, which is time saving and with more optimization degrees of freedom, which can satisfy the requirement of different bandwidth application scenarios. By changing the objective function, the back reflection and polarization dependence problems can also be further optimized.

## REFERENCES

- [1] G. D. Boyd, R. C. Miller, K. Nassau, W. L. Bond, and A. Savage, “LiNbO<sub>3</sub>: An efficient phase matchable nonlinear optical material,” *Appl. Phys. Lett.*, vol. 5, pp. 234–236, Nov. 2004.
- [2] J. Lin, F. Bo, Y. Cheng, and J. Xu, “Advances in on-chip photonic devices based on lithium niobate on insulator,” *Photon. Res.*, vol. 8, pp. 1910–1936, 2020.
- [3] J. Lin et al., “Electro-optic tuning of a single-frequency ultranarrow linewidth microdisk laser,” *Proc. SPIE*, vol. 4, 2022, Art. no. 036001.
- [4] Y. Kong et al., “Recent progress in lithium niobate: Optical damage, defect simulation, and on-chip devices,” *Adv. Mater.*, vol. 32, 2020, Art. no. 1806452.
- [5] C. Wang, M. Zhang, M. Yu, R. Zhu, H. Hu, and M. Loncar, “Monolithic lithium niobate photonic circuits for Kerr frequency comb generation and modulation,” *Nature Commun.*, vol. 10, 2019, Art. no. 978.
- [6] M. Zhang et al., “Ultrahigh-Q lithium niobate microring Resonator,” *Nature*, vol. 568, 2019, Art. no. 373.
- [7] Y. He et al., “Self-starting bi-chromatic LiNbO<sub>3</sub> soliton microcomb,” *Optica*, vol. 6, pp. 1138–1144, 2019.
- [8] Y. Xue et al., “Breaking the bandwidth limit of a high-quality-factor ring modulator based on thin-film lithium niobate,” *Optica*, vol. 9, pp. 1131–1137, 2022.
- [9] C. Wang et al., “Integrated lithium niobate electro-optic modulators operating at CMOS-compatible voltages,” *Nature*, vol. 562, pp. 101–104, 2018.
- [10] L. He, M. Zhang, A. S. Ansari, R. Zhu, C. Wang, and M. Loncar, “Low-loss fiber-to-chip interface for lithium niobate photonic integrated circuits,” *Opt. Lett.*, vol. 44, no. 9, pp. 2314–2317, 2019.
- [11] S. Dizaiin et al., “Self-suspended micro-resonators patterned in Z-cut lithium niobate membranes,” *Opt. Mater. Exp.*, vol. 5, no. 9, pp. 2081–2089, 2015.
- [12] J. Wang et al., “High-Q lithium niobate microdisk resonators on a chip for efficient electro-optic modulation,” *Opt. Exp.*, vol. 23, no. 18, pp. 23072–23078, 2015.
- [13] C. Wang et al., “Integrated high quality factor lithium niobate microdisk resonators,” *Opt. Exp.*, vol. 22, no. 25, pp. 30924–30933, 2014.
- [14] J. Lin et al., “Fabrication of high-Q lithium niobate micro resonators using femtosecond laser micromachining,” *Sci. Rep.*, vol. 5, no. 1, 2015, Art. no. 8072.
- [15] I. Krasnokutska, J. J. Tambasco, X. J. Li, and A. Peruzzo, “Ultra-low loss photonic circuits in lithium niobate on Insulator,” *Opt. Exp.*, vol. 26, no. 2, pp. 897–904, 2018.
- [16] C. Wang et al., “Second harmonic generation in nano-structured thin-film lithium niobate waveguides,” *Opt. Exp.*, vol. 25, no. 6, pp. 6963–6973, 2017.
- [17] Y. Li, T. Lan, J. Li, and Z. Wang, “High-efficiency edge-coupling based on lithium niobate on an insulator wire waveguide,” *Appl. Opt.*, vol. 59, pp. 6694–6701, 2020.
- [18] S. Kang et al., “High-efficiency chirped grating couplers on lithium niobate on insulator,” *Opt. Lett.*, vol. 45, pp. 6651–6654, 2020.
- [19] Z. Chen, Y. Ning, and Y. Xun, “Chirped and apodized grating couplers on lithium niobate thin film,” *Opt. Mater. Exp.*, vol. 10, pp. 2513–2521, 2020.
- [20] I. Krasnokutska, R. Chapman, J. Tambasco, and A. Peruzzo, “High coupling efficiency grating couplers on lithium niobate on insulator,” *Opt. Exp.*, vol. 27, pp. 17681–17685, 2019.
- [21] B. Chen, Z. Ruan, K. Chen, and L. Liu, “One-dimensional grating coupler on lithium-niobate-on-insulator for high-efficiency and polarization-independent coupling,” *Opt. Lett.*, vol. 48, pp. 1434–1437, 2023.
- [22] Z. Ruan et al., “Metal based grating coupler on a thin-film lithium niobate waveguide,” *Opt. Exp.*, vol. 28, pp. 35615–35621, 2020.
- [23] C. M. Lalau-Keraly, S. Bhargava, O. D. Miller, and E. Yablonovitch, “Adjoint shape optimization applied to electromagnetic design,” *Opt. Exp.*, vol. 21, pp. 21693–21701, 2013.
- [24] Z. Lin, A. Pick, M. Lončar, and A. W. Rodriguez, “Enhanced spontaneous emission at third-order Dirac exceptional points in inverse-designed photonic crystals,” *Phys. Rev. Lett.*, vol. 117, 2016, Art. no. 107402.
- [25] L. F. Frellsen, Y. Ding, O. Sigmund, and L. H. Frandsen, “Topology optimized mode multiplexing in silicon-on-insulator photonic wire waveguides,” *Opt. Exp.*, vol. 24, pp. 16866–16873, 2016.
- [26] D. Sell, J. Yang, S. Doshay, R. Yang, and J. A. Fan, “Large-angle, multifunctional metagratings based on freeform multimode geometries,” *Nano Lett.*, vol. 17, pp. 3752–3757, 2017.
- [27] L. Su, A. Y. Piggott, N. V. Sapra, J. Petykiewicz, and J. Vučković, “Inverse design and demonstration of a compact on-chip narrowband three-channel wavelength demultiplexer,” *Nature Photon.*, vol. 9, pp. 374–377, May 2015.
- [28] A. Y. Piggott, J. Petykiewicz, L. Su, and J. Vučković, “Fabrication-constrained nanophotonic inverse design,” *Sci. Rep.*, vol. 7, 2017, Art. no. 1786.
- [29] L. Cai and G. Piazza, “Low-loss chirped grating for vertical light coupling in lithium niobate on insulator,” *J. Opt.*, vol. 21, no. 6, 2019, Art. no. 065801.
- [30] S. Yang et al., “Low loss ridge-waveguide grating couplers in lithium niobate on insulator,” *Opt. Mater. Exp.*, vol. 11, pp. 1366–1376, 2021.
- [31] L. Su, R. Trivedi, N. Sapra, A. Piggott, D. Vercruyse, and J. Vučković, “Fully-automated optimization of grating couplers,” *Opt. Exp.*, vol. 26, pp. 4023–4034, 2018.